

Optical phonons in GaAs/AlAs quantum wires

Shang-Fen Ren and Yia-Chung Chang

*Department of Physics and Materials Research Laboratory, University of Illinois at Urbana-Champaign,
Urbana, Illinois 61801*

(Received 17 December 1990)

Phonon-dispersion curves of semiconductor quantum wires are studied in a realistic rigid-ion model. We introduce an approach for solving the rigid-ion model in quantum wires, which avoids direct computation of the Coulomb interaction. Our calculations demonstrate the interesting anisotropic behavior of long-wavelength optical phonons in quantum wires. In particular, we show that frequencies of several optical phonons approach different values as the wave vector approaches the zone center from three different axes. We have also shown that the lateral confinement in a quantum wire on the interface modes leads to the edge modes.

Recent advances in microfabrication technology have made it possible to grow one-dimensional semiconductors, i.e., quantum wires (QWR's), with controllable geometries and dimensions. These structures have attracted rapidly growing interest in both science and technology in the last few years.¹⁻³ There has been a great deal of theoretical studies on the electronic properties of quantum wires;^{4,5} however, theoretical studies of phonons in these structures have not been reported. Phonons in semiconductor superlattices, on the other hand, have been studied extensively and their behaviors are well understood.⁶⁻²⁴ In this paper we report calculations of phonon dispersion curves of GaAs/AlAs quantum wires using a rigid-ion model. We found that the anisotropic behaviors of optical phonons in quantum wires are more complicated than that in superlattices. The frequencies of certain optical modes can be quite different when the wave vector (\mathbf{k}) approaches zero from all different directions in the three-dimensional space. In contrast, the optical phonons in superlattices are isotropic for wave vectors approaching zero in directions perpendicular to the growth direction. The interface modes which exist in superlattices are modified by the lateral confinement in the quantum wire and turn into laterally confined interface modes or edge modes.

A typical GaAs QWR structure of interest is shown schematically in Fig. 1. In this structure, an array of GaAs quantum wires embedded in AlAs are aligned along the $[\bar{1}10]$ direction with interfaces normal to the $[001]$ and $[110]$ directions. We shall call the $[001]$ and $[110]$ directions which are normal to the interfaces as two lateral directions. Throughout the paper, we use a transformed coordinate system, in which the z direction is along $[001]$, the new x direction along $[110]$, and the new y direction is along $[\bar{1}10]$. The QWR unit cell consists of $(m_1+n_1) \times (m_2+n_2)$ bulk unit cells, out of which $m_1 \times m_2$ are GaAs unit cells and the rest are AlAs unit cells. We shall refer to such a structure as the $(m_1+n_1) \times (m_2+n_2)$ GaAs/AlAs QWR.

A rigid-ion model is used in our calculations. In this model, the polarization in an ionic crystal is determined completely by the displacements of ions (assumed point-like) from their equilibrium positions. The polarization within ions is ignored. The equation of motion for the ionic displacement is given by

$$\sum_{\alpha'} \underline{D}_{\alpha\alpha'}(\mathbf{k}) \underline{U}_{\alpha'} = \omega^2(\mathbf{k}) \underline{M}_{\alpha\alpha} \underline{U}_{\alpha}, \quad (1)$$

where $\underline{D}(\mathbf{k})$ is the dynamic matrix, \underline{M} is the mass matrix, and \underline{U} is the polarization vector. $\alpha, \alpha'=1, \dots, 6$ with the first three components describing the vibrations along the $x, y,$ and z directions for cations and the last three components describing those for anions. The dynamic matrix consists of two parts—the short-range (SR) interaction matrix and the Coulomb (C) interaction matrix:

$$\underline{D}(\mathbf{k}) = \underline{D}^{\text{SR}}(\mathbf{k}) + \underline{C}(\mathbf{k}). \quad (2)$$

Eleven parameters are used to fit the bulk phonon-

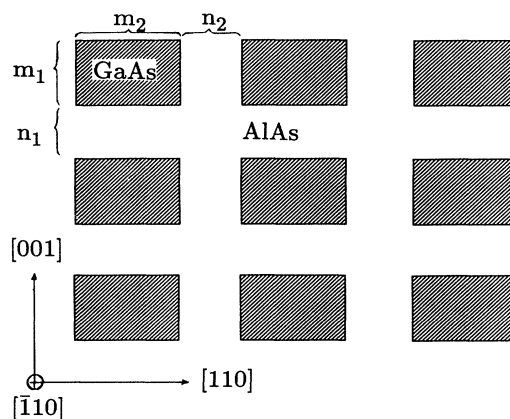


FIG. 1. A schematical diagram for a $(m_1+n_1) \times (m_2+n_2)$ GaAs/AlAs QWR structure.

dispersion curves of the constituent materials (GaAs and AlAs) to the neutron scattering data. The best-fit parameters can be found in Refs. 18, 25, and 26. Recently this model was adopted by Ren, Chu, and Chang to calculate the phonon-dispersion curves of GaAs/AlAs semiconductor superlattices.¹⁸ In adapting the eleven-parameter rigid-ion model to QWR's, we choose the short-range interaction parameters between any two atoms in the QWR's to be the same as those in the corresponding bulk material with the exception that the interaction between a Ga atom and an Al atom across an interface is taken to be the average of the Ga-Ga interaction in bulk GaAs and the Al-Al interaction in bulk AlAs. The present treatment of the long-range Coulomb interaction is different from that used in Ref. 18. In the present approach, we assume that the atomic charge transfers for GaAs and AlAs are the same. This approximation has been used in previous theoretical studies for superlattices,^{17,19} and it is a fairly good approximation for GaAs/AlAs QWR's. In this approximation, the Coulomb interaction in QWR is identical to that in a fictitious QWR made of only one bulk material, of which the phonon modes can be obtained from the folding of the bulk phonon-dispersion curves along two lateral directions. Because now we assume that GaAs and AlAs have the same charge transfer, the difference in phonon-dispersion curves between QWR and the bulk material is caused only by the difference in short-range interactions of GaAs and AlAs and the mass difference between Ga and Al atoms.

The unit cell of a QWR (henceforth defined as a super cell) consists of $N_1 \times N_2$ bulk unit cells with N_1 columns aligned in the [001] direction and N_2 rows aligned in the [110] direction. Each bulk unit cell consists of two atoms (one cation and one anion) separated by a distance vector $\tau = (1, 1, 1)a/4$. For a QWR the equation of motion can be cast into the following matrix equation:

$$\sum_{\mathbf{R}'\alpha'} \langle \mathbf{R}, \alpha | \underline{M}^{-1/2} \underline{D}(\mathbf{k}_s) \underline{M}^{-1/2} | \mathbf{R}'\alpha' \rangle \langle \mathbf{R}'\alpha' | \underline{U}' \rangle = \omega^2(\mathbf{k}_s) \langle \mathbf{R}\alpha | \underline{U}' \rangle. \quad (3)$$

Here \mathbf{R}, \mathbf{R}' run over all position vectors of bulk unit cells in a QWR super cell, and the indices α, α' have the same meaning as in Eq. (1). We have multiplied both sides of the dynamic equation by $\underline{M}^{-1/2}$ to convert the generalized eigenvalue problem to a simple eigenvalue problem. $\underline{U}' \equiv \underline{M}^{1/2} \underline{U}$. The other notations are self-explanatory. The wave vector \mathbf{k}_s is restricted in the first Brillouin zone

of QWR.

For a fictitious QWR made of the material (say GaAs), we denote the corresponding \underline{D} , \underline{M} , and \underline{U}' by \underline{D}_0 , \underline{M}_0 , and $\underline{U}^{(0)}$, respectively. Since the solutions of the fictitious QWR can be obtained by zone folding of the bulk phonon modes, we label the eigenfrequency and polarization vector for the n th folded phonon mode with polarization ν by $\omega_{\nu n}^{(0)}$ and $\underline{U}_{\nu n}^{(0)}$, respectively. They are related to the corresponding bulk phonon frequency and polarization vector by

$$\omega_{\nu n}^{(0)}(\mathbf{k}_s) = \bar{\omega}^{(\nu)}(\mathbf{k}_s + \mathbf{g}_n)$$

and

$$\langle \mathbf{R}\alpha | \underline{U}_{\nu n}^{(0)} \rangle = \frac{1}{\sqrt{N_1 N_2}} e^{i\mathbf{g}_n \cdot \mathbf{R}} \bar{\underline{U}}_{\alpha}^{(\nu)}(\mathbf{k}_s + \mathbf{g}_n),$$

where \mathbf{g}_n denotes the n th QWR reciprocal lattice vector; $n = 1, \dots, N_1 \times N_2$. $\bar{\omega}^{(\nu)}(\mathbf{k})$ and $\bar{\underline{U}}^{(\nu)}(\mathbf{k})$ denote the eigenfrequency and polarization vector, respectively, of the ν th bulk phonon mode at wave vector \mathbf{k} (\mathbf{k} is now restricted in the first Brillouin zone of a bulk material). The equation of motion for the fictitious QWR is given by

$$\sum_{\mathbf{R}'\alpha'} \langle \mathbf{R}\alpha | \underline{M}_0^{-1/2} \underline{D}_0(\mathbf{k}_s) \underline{M}_0^{-1/2} | \mathbf{R}'\alpha' \rangle \langle \mathbf{R}'\alpha' | \underline{U}_{\nu n}^{(0)} \rangle = \omega_{\nu n}^{(0)2}(\mathbf{k}_s) \langle \mathbf{R}\alpha | \underline{U}_{\nu n}^{(0)} \rangle. \quad (4)$$

Using the completeness relation

$$\sum_{\nu n} \langle \mathbf{R}\alpha | \underline{U}_{\nu n}^{(0)} \rangle \langle \underline{U}_{\nu n}^{(0)} | \mathbf{R}\alpha' \rangle = \delta_{\mathbf{R}, \mathbf{R}'} \delta_{\alpha, \alpha'},$$

we convert Eq. (3) (via a unitary transformation) into

$$\sum_{\nu n'} \langle \nu n | \underline{M}^{-1/2} \underline{D}(\mathbf{k}_s) \underline{M}^{-1/2} | \nu' n' \rangle \langle \nu' n' | \underline{U}' \rangle = \omega^2(\mathbf{k}_s) \langle \nu n | \underline{U}' \rangle, \quad (5)$$

where we have used the abbreviated notation $|\nu n\rangle$ for $|\underline{U}_{\nu n}^{(0)}\rangle$.

Now we write $\underline{D} = \underline{D}_0 + \Delta \underline{D}^{\text{SR}}$, where $\Delta \underline{D}^{\text{SR}} = \underline{D}^{\text{SR}} - \underline{D}_0^{\text{SR}}$. Note that the Coulomb part is completely absorbed in \underline{D}_0 , since it is the same for the superlattice and the fictitious superlattice made of bulk GaAs. Substituting Eq. (4) into Eq. (5) yields

$$\sum_{\nu' n'} (\langle \nu n | \Omega | \nu' n' \rangle + \langle \nu n | \underline{M}^{-1/2} \Delta \underline{D}^{\text{SR}} \underline{M}^{-1/2} | \nu' n' \rangle) \langle \nu' n' | \underline{U}' \rangle = \omega^2(\mathbf{k}_s) \langle \nu n | \underline{U}' \rangle, \quad (6)$$

where

$$\langle \nu n | \Omega | \nu' n' \rangle \equiv \sum_{\nu'' n''} \langle \nu n | \underline{M}^{-1/2} \underline{M}_0^{1/2} | \nu'' n'' \rangle \omega_{\nu'' n''}^{(0)2}(\mathbf{k}_s) \langle \nu'' n'' | \underline{M}_0^{1/2} \underline{M}^{-1/2} | \nu' n' \rangle.$$

The above eigenvalue problem can be solved numerically to get the QWR phonon frequencies. This method avoids the specific treatment of the Coulomb interaction for QWR because it is already included in the zeroth-order dynamic matrix \underline{D}_0 . This method can also be used to treat phonons in superlattices, and the results are identical to those obtained by the method used in Ref. 18, provided the Coulomb interaction parameters for GaAs and AlAs are taken to be the same. The method is, in a certain sense, similar to that used by Huang and Zhu.²¹ However, the method introduced here takes into account the short-range interactions exactly within the rigid-ion model. This is of importance for treating superlattices and quantum wires with short periods.

We have calculated phonon frequencies of QWR for wave vectors propagating in different directions. One of the most interesting results of phonons in QWR is the anisotropic behavior of optical phonons near the zone center. That is, for certain optical modes, the frequencies near the zone center are different when $\mathbf{k} \rightarrow 0$ from different directions. Figure 2 shows the results of near-zone-center GaAs-like optical-phonon frequencies of a $(2+2) \times (3+3)$ GaAs/AlAs QWR as functions of the angle of orientation of the wave vector. The charge-transfer parameter (Q) used in obtaining these results is taken to be the same as in bulk GaAs. The angle of orientation of the wave vector is defined as (θ, ϕ) with θ being the polar angle and ϕ being the azimuthal angle in the transformed coordinate system. In the left panel, the wave vector is rotating from the z axis to the x axis in the z - x plane (perpendicular to the direction of quantum wire), i.e., $\theta = 0 \rightarrow \pi/2$ and $\phi = 0$. In the middle panel the wave vector is rotating from the x axis to the y axis in the x - y plane, i.e., $\theta = \pi/2$ and $\phi = 0 \rightarrow \pi/2$. In the right panel the wave vector is rotating from the y axis back to the z axis in the y - z plane, i.e., $\theta = \pi/2 \rightarrow 0$ and $\phi = \pi/2$. The values of θ and ϕ are displayed along the bottom

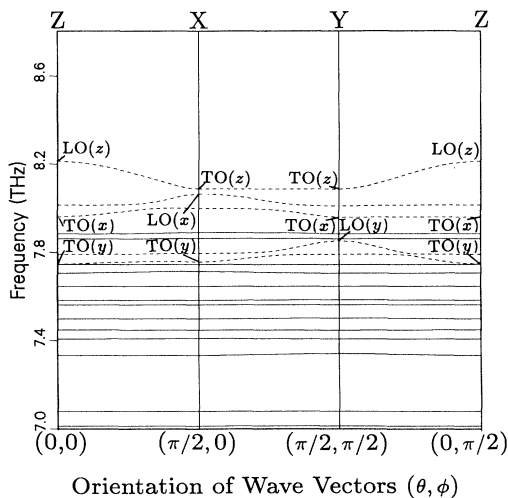


FIG. 2. Angular dispersion of GaAs-like long-wavelength optical modes for a $(2+2) \times (3+3)$ GaAs/AlAs QWR.

axes of Fig. 2. The dashed curves are for modes with large angular dispersion and the solid lines are for modes with weak or zero angular dispersion.

Various features of the anisotropy of optical phonons in superlattices have been described in Ref. 18, e.g., only the principal modes (modes with a nodeless envelope function) can have significant angular dispersion, while the other modes are nearly angular dispersionless except when they are mixed with a principal mode at a certain angle where their frequencies tend to cross each other. In analyzing the GaAs-like QWR phonons, we notice that if we ignore the anticrossing effect there are three branches which have substantial angular dispersion. These three branches are actually three principal modes derived from one bulk longitudinal mode and two bulk transverse modes. At $(\theta, \phi) = (0, 0)$, the longitudinal mode is predominantly z -like and the two transverse modes are predominantly x -like and y -like. Thus, we mark them as $LO(z)$, $TO(x)$, and $TO(y)$. Because of the confinement effect from both the z and x directions, these modes do not have pure polarization. This is in contrast with the superlattice case. At $(\theta, \phi) = (\pi/2, 0)$, the longitudinal mode is predominantly x -like and the two transverse modes are predominantly z -like and y -like. We therefore label these modes $LO(x)$, $TO(z)$, and $TO(y)$. Similarly, at $(\theta, \phi) = (\pi/2, \pi/2)$, we mark the three principal modes by $LO(y)$, $TO(z)$, and $TO(x)$. In the left panel, the wave vector lies in the z - x plane, so the frequency of the $TO(y)$ mode remains nearly constant as seen in Fig. 2. Similarly, in the middle panel the $TO(z)$ frequency remains nearly constant and in the right panel the $TO(x)$ frequency remains nearly constant. In each of the three panels, an LO mode and a TO mode tend to couple with each other as the direction of wave vector deviates from the symmetry axes. This results in angular dispersion of the two coupled modes. For example, in the left panel the $LO(z)$ frequency decreases and the $TO(x)$ increases as θ increases and their frequencies become very close at $\theta = \pi/2$. For $0 < \theta < \pi/2$, each of the modes contains strong admixture of x and z components. When θ reaches $\pi/2$, the z -like mode becomes a transverse mode and the x -like mode becomes a longitudinal mode. Similar behavior is seen for phonon dispersion in the middle and right panels with the roles played by the x -, y -, and z -like modes changed.

Similar to the optical anisotropy of superlattices the optical anisotropy in QWR can be understood as follows. In the long-wavelength limit, the long-range Coulomb interaction in a bulk material can be written as

$$C_{i,j}(\mathbf{k}, \sigma, \sigma') = 4\pi \left(\frac{Q_\sigma Q_{\sigma'}}{v} \right) \left(\frac{k_i k_j}{k^2} - \frac{1}{3} \delta_{ij} \right), \quad (7)$$

where i, j denote the x, y, z directions, σ and σ' denote atomic species (cation or anion), Q_σ denotes the charge transfer of atomic species σ , and v is the volume of the bulk unit cell. It is noted that the matrix elements of the long-range Coulomb interaction have an angular dependence from the term $k_i k_j / k^2$. This leads to

angle-dependent polarization vectors when \mathbf{k} approaches zero from different directions. However, the zone-center phonon frequencies remain angle independent, since the bulk material has cubic symmetry. The same description can be used for the phonon modes of a fictitious QWR made of the same bulk material. However, for a QWR the angle of orientation is referred to \mathbf{k}_s (restricted in the QWR Brillouin zone) rather than \mathbf{k} . For the n th folded phonon mode, the QWR polarization vector is given by the bulk polarization vector at $\mathbf{k} = \mathbf{k}_s + \mathbf{g}_n$. In the limit $k_s \rightarrow 0$, $\mathbf{k} = \mathbf{k}_s$ for the principal mode ($\mathbf{g}_n = 0$) and $\mathbf{k} = \mathbf{g}_n$ otherwise. Thus, for the principal modes the polarization vectors are angle dependent, whereas for the folded modes ($\mathbf{g}_n \neq 0$) the polarization vectors are angle independent.

Now, we consider a realistic QWR. In our treatment we simply add the differences in short-range dynamic matrices and in the atomic masses to the fictitious QWR. The resulting phonon frequencies for the principal modes will be angle dependent, since the perturbation matrices are evaluated in an angle-dependent basis and the perturbation does not have cubic symmetry. The folded modes ($\mathbf{g}_n \neq 0$), on the other hand, do not have angular dispersion unless they are coupled to the principal modes via the perturbation. The coupling is non-negligible when their frequencies are close to each other as seen in Fig. 2.

The same argument applies to semiconductor superlattices. For a superlattice grown along the [001] direction, the material does not have cubic symmetry but it is still symmetric with respect to the exchange of x and y coordinates. Consequently the zone-center principal modes will exhibit angular dispersion for \mathbf{k}_s rotating from the z direction to any directions in the x - y plane. However, no angular dispersion occurs for \mathbf{k}_s rotating in the x - y plane. In contrast, the principal optical modes of the semicon-

ductor QWR have angular dispersion for any direction of orientation of \mathbf{k}_s as a result of lower symmetry.

It is instructive to compare the anisotropic behavior of optical phonons in quantum wires to that in related superlattices. The $(2+2) \times (3+3)$ GaAs/AlAs QWR discussed above can be constructed from a (001)-grown $(\text{GaAs})_2$ - $(\text{AlAs})_2$ superlattice by replacing every three out of six columns of GaAs arrays normal to the [110] direction with AlAs arrays. Alternatively, it can be constructed from a (110)-grown $(\text{GaAs})_3$ - $(\text{AlAs})_3$ superlattice by replacing every two out of four rows of GaAs arrays normal to the [001] direction with AlAs arrays. Figures 3 and 4 show the angular dispersion of GaAs-like optical phonons of an (001) $(\text{GaAs})_2$ - $(\text{AlAs})_2$ superlattice and that of a (110) $(\text{GaAs})_3$ - $(\text{AlAs})_3$ superlattice. We have artificially enlarged the unit cell of these superlattices to the same dimension as the super cell of the QWR. This way we obtain folded phonon bands of the superlattices which are intimately related to the QWR phonon bands. The anisotropic behaviors of the superlattices follow the description given in the previous paragraph. It is noted that the angular dispersion is much stronger in the superlattices than in QWR. The highest GaAs-like phonon frequencies in the (001) and (110) superlattices are around 8.5 and 8.7 THz, respectively. They correspond to the frequencies of the confined LO phonon principal modes. The corresponding confined LO phonon principal mode frequency in QWR is only around 8.2 THz (see Fig. 2), indicating a much stronger confinement in QWR than that in superlattices.

Figure 5 shows the results of near-zone-center AlAs-like optical-phonon frequencies of a $(2+2) \times (3+3)$ AlAs/GaAs QWR as functions of the angle of orientation of the wave vector. This structure is just the QWR structure considered in Fig. 2, but with all the GaAs and AlAs elements exchanged. The charge-transfer pa-

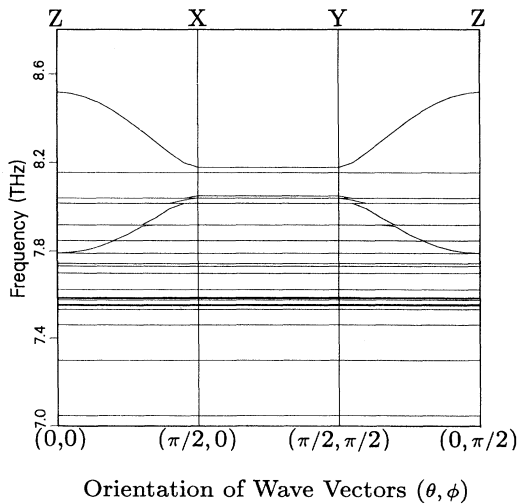


FIG. 3. Angular dispersion of GaAs-like long-wavelength optical modes for a $(\text{GaAs})_2$ - $(\text{AlAs})_2$ (001) superlattice treated as a $(2+2) \times (3+3)$ GaAs/AlAs QWR.

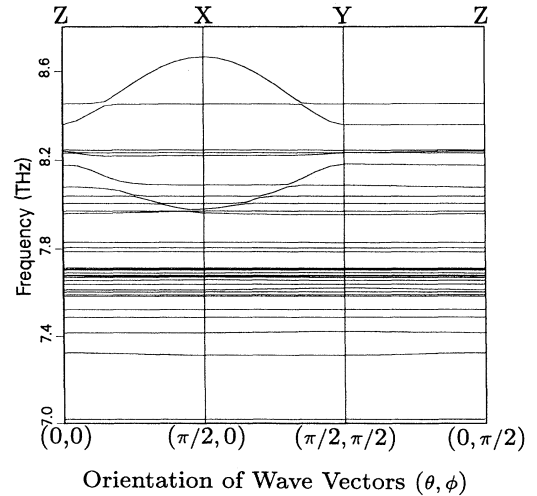


FIG. 4. Angular dispersion of GaAs-like long-wavelength optical modes for a $(\text{GaAs})_3$ - $(\text{AlAs})_3$ (110) superlattice treated as a $(2+2) \times (3+3)$ GaAs/AlAs QWR.

parameter (Q) used in obtaining these results is taken to be the same as in bulk AlAs. Again, we observe angular dispersion in three-dimensional space similar to what we found in Fig. 2. For the AlAs-like modes shown here, we found strong mixing between different branches. For example, for (θ, ϕ) going from $(0, 0)$ to $(\pi/2, 0)$, the LO(z) mode turns into the TO(z) mode with its frequency reduced, while the TO(x) mode turns into the LO(x) mode with its frequency increased. The two branches anticross near $\theta = \pi/4$ with a strong interaction. The angular dispersion of the two branches also affects the dispersion of other branches substantially as can be seen in this figure.

Figure 6 shows phonon frequencies of AlAs-like optical modes for a $(6+6) \times (4+4)$ AlAs/GaAs QWR as functions of the wave vector along the $[\bar{1}10]$ direction (k_y). In order to identify the physical origin of these modes, we compare them with the AlAs-like optical modes in the related GaAs/AlAs superlattices. As we discussed above, we may consider the $(6+6) \times (4+4)$ AlAs/GaAs QWR to be constructed from a $(\text{GaAs})_6-(\text{AlAs})_6$ (001) superlattice or a $(\text{GaAs})_4-(\text{AlAs})_4$ (110) superlattice by substituting AlAs with GaAs at appropriate sites.

First, consider the relation between the QWR and the (001) superlattice. The wave vector k_y (along $[\bar{1}10]$) is a good quantum number in both systems, which will be fixed. The wave vector q_z (along [001]) defined in the superlattice Brillouin zone is also a good quantum number in both systems, since they both have the same periodicity in the [001] direction. Thus, q_z will also be fixed, and we choose $q_z = 0$. However, along the [110] direction the wave vector k_x is a good quantum number in the (001) superlattice, but not in the QWR. Superlattice modes with k_x 's differed by any QWR reciprocal lattice vector in the [110] direction will be mixed to form a QWR mode. Thus, most QWR modes are related to the zone-folded superlattice modes and others are either some kind

of interface modes or edge modes. The interface modes should be localized at the new interfaces introduced in the QWR, i.e., the (110) interfaces for this case. Note that the (001) interfaces which already exist in the (001) superlattices are not counted here, since they do not represent a perturbation in going from the superlattice to the QWR. The interface modes of the (001) superlattice become the zone-folded (or laterally confined) (001) interface modes in the QWR, and their frequencies will fall within the interface bands of the (001) superlattice. Here, the interface bands are dispersion curves of interface modes of the (001) superlattice along the k_x direction. On the other hand, the frequencies of the (110) interface modes will fall into neither the interface bands of the (001) superlattice nor any bulk phonon bands.

This is demonstrated in Fig. 7 in which we superpose the dispersion curves of AlAs-like optical modes of the $(6+6) \times (4+4)$ AlAs/GaAs QWR on the projected phonon bands of a $(\text{GaAs})_6-(\text{AlAs})_6$ (001) superlattice. The projected phonon bands are obtained by the phonon frequencies of the (001) superlattice for many different values of k_x as functions of k_y . The dashed curves are the QWR modes which do not fall into the superlattice projected phonon bands which include projected bulk bands and the superlattice interface bands. These modes are identified as either laterally confined (110) interface modes or edge modes.

Next, we consider the relation between the QWR with

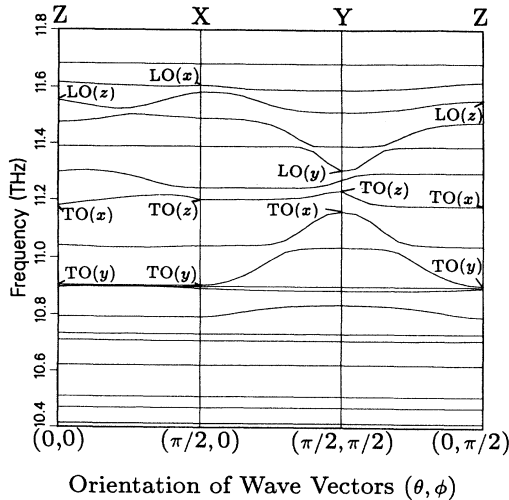


FIG. 5. Angular dispersion of AlAs-like long-wavelength optical modes for a $(2+2) \times (3+3)$ AlAs/GaAs QWR.

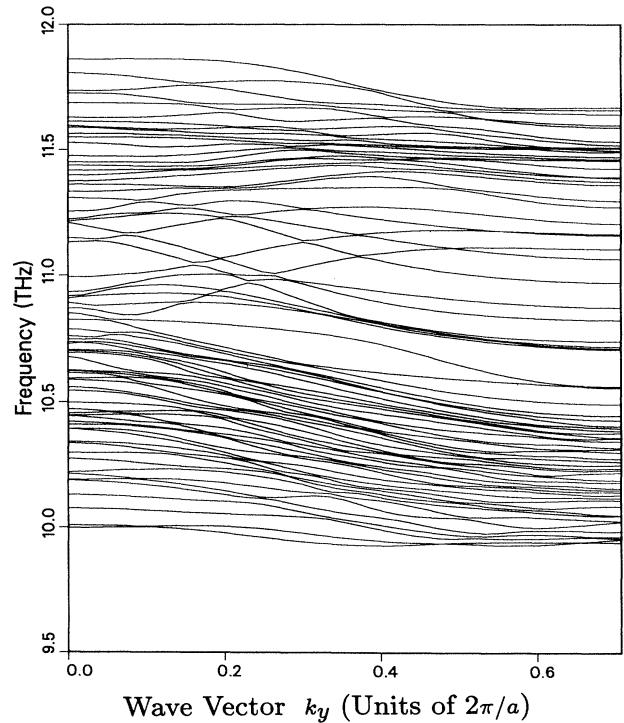


FIG. 6. Dispersion curves of AlAs-like optical modes for a $(6+6) \times (4+4)$ AlAs/GaAs QWR.

a $(\text{GaAs})_4\text{-(AlAs)}_4$ (110) superlattice. The discussions given above also applies here. Now, the laterally confined (110) interface modes will fall within the interface bands of the (110) superlattice, while the laterally confined (001) interface modes or edge modes will not. Figure 8 shows the superposition of the dispersion curves of AlAs-like optical modes of the $(6+6)\times(4+4)$ AlAs/GaAs QWR on the projected phonon bands of a $(\text{GaAs})_4\text{-(AlAs)}_4$ (110) superlattice. The dashed curves are the QWR modes which do not fall into the superlattice projected phonon bands. These modes are either laterally confined (001) interface modes or edge modes.

To separate out the edge modes from the laterally confined interface modes, we superpose the dispersion curves of AlAs-like optical modes of the $(6+6)\times(4+4)$ AlAs/GaAs QWR on projected phonon bands from both the (001) and (110) superlattices. This is shown in Fig. 9. The dashed curves are now identified as the edge modes. We identified four edge modes, presumably corresponding to linear combinations of the four modes localized at the four edges. The problem of edge modes was discussed previously by Maradudin *et al.*²⁷ They considered the long-wavelength acoustic modes of real crystals with edges, corners, and steps. We note that the edge modes are due to the assumed rectangular geometry of the quantum wire and they will be absent in the case of cylindrical wire. In practice, the structures are somewhere between these two extremes.

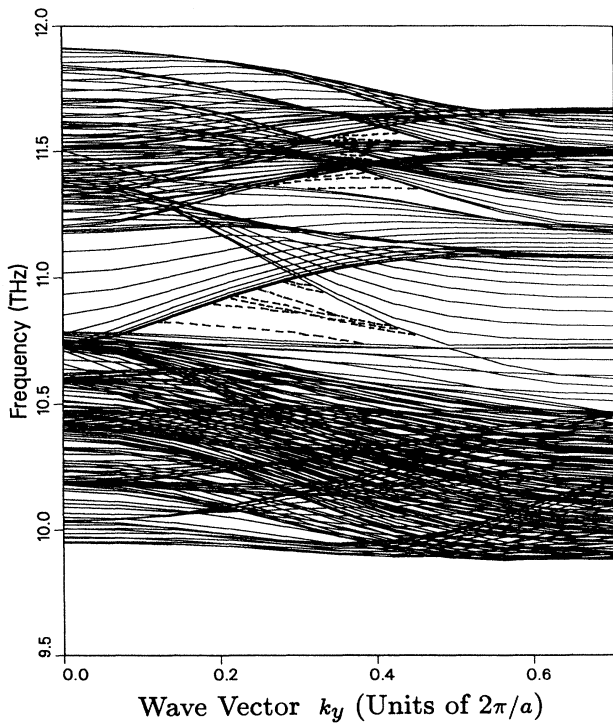


FIG. 7. Dispersion curves of AlAs-like optical modes for a $(6+6)\times(4+4)$ AlAs/GaAs QWR superposed on the projected phonon bands of a $(\text{GaAs})_6\text{-(AlAs)}_6$ (001) superlattice.

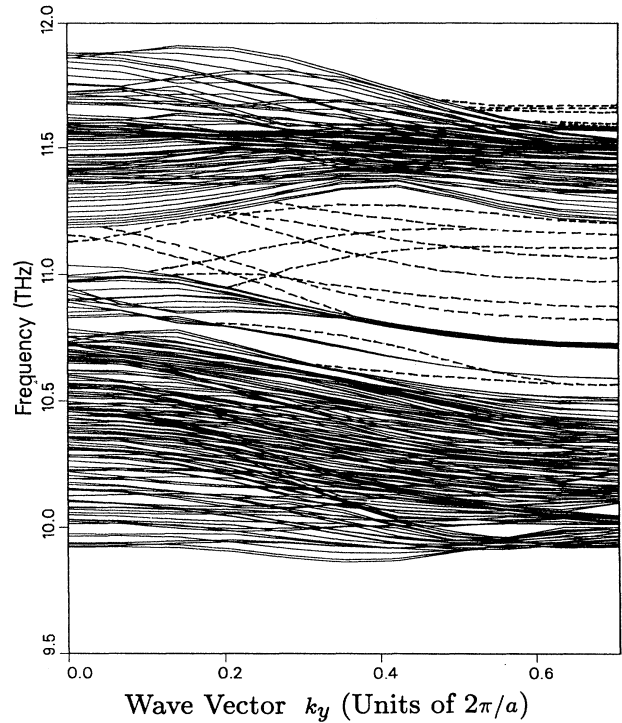


FIG. 8. Dispersion curves of AlAs-like optical modes for a $(6+6)\times(4+4)$ AlAs/GaAs QWR superposed on the projected phonon bands of a $(\text{GaAs})_4\text{-(AlAs)}_4$ (110) superlattice.

In summary, we have calculated the long-wavelength optical phonons in QWRs propagating in all directions in three dimension. We found that in the long-wavelength limit, the optical phonons of QWR's have very unique three-dimensional anisotropic behaviors. We have also studied the dispersion curves of the AlAs-like laterally

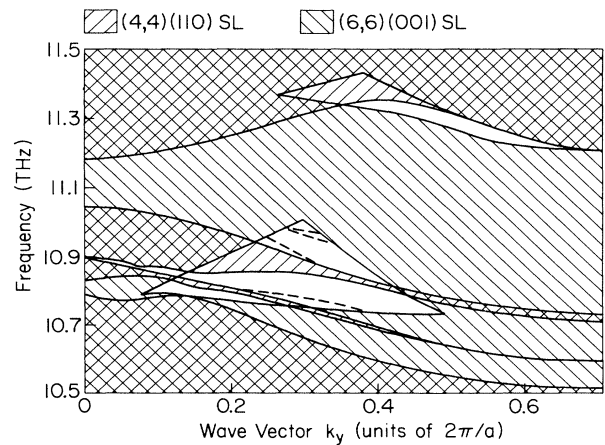


FIG. 9. Dispersion curves of AlAs-like optical modes for a $(6+6)\times(4+4)$ AlAs/GaAs QWR superposed on the projected phonon bands of both the $(\text{GaAs})_6\text{-(AlAs)}_6$ (001) superlattice and the $(\text{GaAs})_4\text{-(AlAs)}_4$ (110) superlattice.

confined interface modes and edge modes. We have not discussed the lateral confinement of GaAs-like interface modes and the GaAs-like edge modes. This is because the projected phonon bands of GaAs/AlAs superlattices do not have a well-defined gap which makes the identification of interface or edge modes difficult. We hope that our calculations will stimulate more experimental measurements and lead to better understanding of semi-

conductor microscopic structures.

This work was supported in part by the U.S. Office of Naval Research (ONR) under Contract No. N00014-89-J-1157. We acknowledge fruitful discussions with H. Chu. We acknowledge the use of the Cray Y-MP supercomputer at the National Center for Supercomputer Applications at University of Illinois.

-
- ¹I. Suemune and L. A. Coldren, *IEEE J. Quantum Electron.* **QE-24**, 1778 (1988).
- ²M. Tsuchiya, J. M. Gaines, R. H. Yan, R. J. Simes, P. O. Holtz, L. A. Coldren, and P. M. Petroff, *Phys. Rev. Lett.* **62**, 466 (1989).
- ³N. C. Constantinou and B. K. Ridley, *Phys. Rev. B* **41**, 10 622 (1990); **41**, 10 627 (1990).
- ⁴J. Xia and K. Huang, *Chin. J. Semicond.* **8**, 1062 (1988).
- ⁵D. S. Citrin and Y. C. Chang, *Phys. Rev. B* **40**, 5507 (1989); *J. Appl. Phys.* **68**, 161 (1990).
- ⁶J. L. Merz, A. S. Barker, Jr., and A. C. Gossard, *Appl. Phys. Lett.* **31**, 117 (1977).
- ⁷A. S. Barker, Jr., J. L. Merz, and A. C. Gossard, *Phys. Rev. B* **17**, 3181 (1978).
- ⁸C. Colvard, R. Merlin, M. V. Klein, and A. C. Gossard, *Phys. Rev. Lett.* **45**, 298 (1980).
- ⁹R. Merlin, C. Colvard, M. V. Klein, H. Morkoç, A.Y. Cho, and A.C. Gossard, *Appl. Phys. Lett.* **36** (1), 43 (1980).
- ¹⁰E. P. Pokatilov and S. L. Beril, *Phys. Status Solidi B* **118**, 567 (1983).
- ¹¹M. Babiker, *J. Phys. C* **19**, 683 (1986); *Physica B+C* **145B**, 111 (1987).
- ¹²E. P. Fuchs and K. L. Kliewer, *Phys. Rev.* **140**, A2076 (1965).
- ¹³S. M. Rytov, *Zh. Eksp. Teor. Fiz.* **29**, 605 (1956) [*Sov. Phys.—JETP* **2**, 466 (1956)].
- ¹⁴R. Enderlin, F. Bechstedt, and G. Gerecke, *Phys. Status Solidi B* **148**, 173 (1988).
- ¹⁵S. K. Yip and Y. C. Chang, *Phys. Rev. B* **30**, 7037 (1984).
- ¹⁶A. Kobayashi, Ph.D. thesis, University of Illinois at Urbana-Champaign, 1985.
- ¹⁷T. Toriyama, N. Kobayashi, and Y. Horikoshi, *Jpn. J. Appl. Phys.* **25**, 1895 (1987).
- ¹⁸S.-F. Ren, H. Chu, and Y. C. Chang, *Phys. Rev. Lett.* **59**, 1841 (1987); *Phys. Rev. B* **37**, 8899 (1988).
- ¹⁹E. Richter and D. Strauch, *Solid State Commun.* **46**, 867 (1987).
- ²⁰H. Chu, S.-F. Ren, and Y. C. Chang, *Phys. Rev. B* **37**, 10 746 (1988).
- ²¹K. Huang and B. Zhu, *Phys. Rev. B* **38**, 2183 (1988); **38**, 13 377 (1988).
- ²²B. Zhu, *Phys. Rev. B* **38**, 7694 (1988).
- ²³T. Tsuchiya, H. Akera, and T. Ando, *Phys. Rev. B* **39**, 6025 (1989).
- ²⁴A. Fasolino, E. Molinari, and J. C. Maan, *Superlatt. Microstruct.* **3**, 117 (1987).
- ²⁵K. Kunc, *Ann. Phys. (France)* **8**, 319 (1973-1974).
- ²⁶K. Kunc, M. Balkanski, and M. Nusimovici, *Phys. Status Solidi B* **72**, 229 (1975).
- ²⁷A. A. Maradudin, R. F. Wallis, D. L. Mills, and R. L. Ballard, *Phys. Rev. B* **6**, 1106 (1972).